*Geological Magazine*

**www.cambridge.org/geo**

# Fluctuation in redox conditions and the evolution of early Cambrian life constrained by nitrogen isotopes in the middle Yangtze Block, South China

Kai Wei[1,5], Hansheng Cao[2,3,4], Fajin Chen[2,3,4], Zaiyun Wang[2,3,4], Zhihui An[1,5], Hanli Huang[2,3,4] and Chunqing Chen[2,3,4]

[1]Wuhan Center, China Geological Survey (Geosciences Innovation Center of Central South China), Wuhan, China; [2]Laboratory for Coastal Ocean Variation and Disaster Prediction, College of Ocean and Meterology, Guangdong Ocean University, Zhanjiang, China; [3]Key Laboratory of Climate, Resources and Environment in Continental Shelf Sea and Deep Sea of Department of Education of Guangdong Province, College of Ocean and Meteorology, Guangdong Ocean University, Zhanjiang, China; [4]Key Laboratory of Space Ocean Remote Sensing and Application, Ministry of Natural Resources, Beijing, China and [5]Hubei Key Laboratory of Paleontology and Geological Environment Evolution, Wuhan Center of China Geological Survey, Wuhan, China

**Original Article**

**Cite this article:** Wei K, Cao H, Chen F, Wang Z, An Z, Huang H, and Chen C (2023) Fluctuation in redox conditions and the evolution of early Cambrian life constrained by nitrogen isotopes in the middle Yangtze Block, South China. *Geological Magazine* **160**: 1932–1945. https://doi.org/10.1017/S0016756823000833

Received: 18 July 2023
Revised: 12 October 2023
Accepted: 2 December 2023
First published online: 18 January 2024

**Keywords:**
Carbon isotope anomalies; Cambrian explosion; nitrogen cycling; Paleo-oceanic environment; nitrate pool

**Corresponding author:**
Hansheng Cao; Email: chsheng72@163.com

## Abstract

The Ediacaran–Cambrian (E-C) transition (~542–517 Ma) witnessed the rapid evolution of Cambrian animals, which was accompanied by carbon cycling anomalies and a significant increase in the concentration of oxygen in Earth's atmosphere. The mechanisms stimulating the evolution of complex eukaryotes, however, remain problematic, especially concerning the link between biological evolution and contemporaneous changes in the oceanic environment. In this study, integrated $\delta^{13}C_{carb}$–$\delta^{13}C_{org}$–$\delta^{15}N$ compositions were analysed from the YD-4 core samples to understand redox fluctuations and nitrogen cycling of the middle Yangtze Block across the E-C transition. Two negative $\delta^{13}C_{carb}$ excursions (N1 and N2) and a positive $\delta^{13}C_{carb}$ excursion (P1) are identified from the studied samples and are supposedly of primary origin. Constrained by of the U-Pb age, biolithology and pattern of isotopic variation, N1, P1 and N2 are comparable to the Basal Cambrian Carbon Isotope Excursion (BACE), Zhujiaqing Carbon Isotope Excursion (ZHUCE) and Shiyantou Carbon Isotope Excursion (SHICE). We interpreted the decreased $\delta^{15}N$ values in this study as resulting from intensified atmospheric nitrogen fixation driven by enhanced denitrification associated with expanded marine anoxia, as well as partial ammonium assimilation, while increased $\delta^{15}N$ values suggest weakened denitrification associated with an amplified oxic water mass. The temporal coincidence of N1 and N2, with two episodes of negative $\delta^{15}N$ excursions, and of P1, with a positive $\delta^{15}N$ excursion, suggests that variable oceanic redox conditions and nitrogen bioavailability may have influenced the evolution of the Cambrian eukaryote-dominated community.

## 1. Introduction

The transition between the terminal Ediacaran and early Cambrian at ca. 542–517 Ma recorded an unprecedented biological evolution event on Earth, namely, the 'Cambrian explosion', resulting in the rapid diversification of metazoans during this period (Marshall, 2006; Erwin *et al.* 2011). The Cambrian explosion encompassed a series of episodic radiations. For example, the extinction of Ediacaran fauna occurred near the Ediacaran–Cambrian (E-C) boundary (Laflamme *et al.* 2013) and small shelly fauna (SSF), which are represented by the Meishucun Biota and Tommotiid, flourished in the Meishucun stage from ca. 539–521 Ma (Li *et al.* 2007; Zhuravlev & Wood, 2018). Afterwards, small shelly biota disappeared in the late Meishucun stage; then, Cambrian biota, represented by the Chengjiang biota of the Qiongzhusi stage, increased rapidly at ca. 521–515 Ma (Chen, 2009; Fu *et al.* 2019).

Investigation of the chemical environment of the ocean is an important basis for understanding the cause of the radiation of paleontological species, and among them, the reconstruction of redox conditions in the paleo-ocean is a key point. At present, there exist three hypotheses regarding the coevolutionary relationship between oxygenation events and the explosion of Cambrian life: the radiation of Cambrian life caused by a globally oxygenated atmosphere–marine system (Canfield *et al.* 2008; Fu *et al.* 2019), complete oceanic oxidation induced by Cambrian fauna and phytoplankton-induced evolution (Lenton *et al.* 2014; Xiao, 2012) and no causal relationship (Mills & Canfield, 2014). In past studies, redox-sensitive elements (e.g., U, V, Mo) and Fe species have been extensively used to show the redox structures in local bottom waters (Algeo & Tribovillard, 2009; Chang *et al.* 2018; Li *et al.* 2020); however,

there are also limitations in applying these parameters (Algeo & Li, 2020; Liu *et al.* 2020). For example, the validity of Fe speciation has been questioned (Clarkson *et al.* 2014), especially in the context of total Fe contents <0.5% (Fan *et al.* 2018). As a limiting nutrient for organisms, nitrogen has remarkably different biogeochemical cycling processes and fractionation effects under different redox conditions. Since the biogeochemical process of nitrogen is sensitive to biological activities in the photic zone, the nitrogen isotope information retained in sedimentary organic matter can more effectively reveal the redox conditions of water and the position of the chemocline, as well as paleoproductivity levels (Canfield *et al.* 2010; Devol, 2015; Zhu *et al.* 2021; Wu *et al.* 2022). Thus, the application of nitrogen isotopes to determine the marine redox environment has distinct advantages over other common parameters, such as redox-sensitive elements and Fe species. At present, nitrogen isotope studies are increasingly being used in studies of redox conditions in South China; however, the majority of these studies focus on the lower Yangtze Block, which comprises massive shallow-water carbonate facies and basinal facies deposits (Xiaotan in Yunnan, Dingtai in Guizhou, Daotuo in Guizhou, Yinjiang in Guizhou and Yuanjia in Hunan) (Cremonese *et al.* 2013; Wei *et al.* 2017; Chen *et al.* 2019; Wu *et al.* 2022). The middle Yangtze Block sedimentary rocks that record a pattern of the nitrogen cycle within the E-C transition are still less investigated, particularly in the transitional facies; thus, nitrogen isotope studies in this region enable us to more clearly depict the redox structure of the early Cambrian Yangtze Ocean.

To reveal the biogeochemical processes related to the nitrogen cycle process and further unravel the links between environmental changes and early metazoan evolution, we conducted time series measurements of carbon isotopes of the carbonate samples ($\delta^{13}C_{carb}$), organic carbon isotopes ($\delta^{13}C_{org}$) and bulk nitrogen isotopes ($\delta^{15}N$) from a deep borehole in the middle Yangtze Block.

## 2. Geological setting

The South China Craton was located at approximately 30°N during the early Cambrian (Fig. 1a) and is composed of the Yangtze Block and the Cathaysia Block (Fig. 1b). As a result of the Neoproterozoic rifting event at approximately 820 Ma, the Yangtze Block progressively converted from a single rift basin to a continental margin basin spreading from northwest to southeast during the early Cambrian (Wang & Li, 2003); this conversion led to the development of three different depositional patterns, namely, shallow-water platform facies, transition facies and slope-basin facies (Jiang *et al.* 2012; Gao *et al.* 2016) (Fig. 1b). In terms of sedimentary sequences during the E-C transition, the shallow-water facies was dominated by carbonate deposits (e.g., the Dengying and Zhujiajing formations), and the mid- and deep-water slope basin facies were predominantly characterized by siliciclastic deposits (e.g., the Liuchapo and Laopu formations) (Och *et al.* 2016). During Cambrian Stages 2–3, a series of black shales were extensively formed throughout the Yangtze Block under the context of global sea level rise (e.g., Shuijingtuo and Qiongzhusi formations) (Jin *et al.* 2020; Chen *et al.* 2022).

In this study, samples were obtained from the YD-4 core on the southern edge of the Huangling Uplift in the middle Yangtze Block and were formed in deep shelf palaeogeographical conditions (Chen *et al.* 2018; Zhang *et al.* 2019). Lithostratigraphically, the E-C transition in the study area includes the Dengying, Yanjiahe and Shuijingtuo formations. Among them, the Dengying Formation is mainly composed of dolomite. The Yanjiahe Formation unconformably overlies the Dengying Formation and is composed of dolomite, calcareous shale, limestone and chert. The Shuijingtuo Formation is in conformable contact with the underlying Yanjiahe Formation and mainly consists of organic-rich shale, argillaceous limestone and limestone lenses.

## 3. Materials and methods

In this study, 47 samples were taken from the YD-4 borehole (1283–1373 m, coordinates: 11°20′55.5″, 30°18′41.0″) that penetrates the Dengying Formation, Yanjiahe Formation and the lower part of the Shuijingtuo Formation. We measured samples for $\delta^{13}C_{carb}$ and oxygen isotopes of carbonate ($\delta^{18}O$), $\delta^{13}C_{org}$, $\delta^{15}N$, as well as the carbonate weight percent, total organic carbon (TOC) and total nitrogen (TN) abundances at the Laboratory for Coastal Ocean Variation and Disaster Prediction of Guangdong Ocean University, China. Concentrations of trace elements were analysed at the Central South Mineral Resources Supervision and Testing Center of the Ministry of Natural Resources (Wuhan, China).

Sample powders (~1 mg) were subjected to a 24-hour reaction with 100% phosphoric acid to measure the $\delta^{13}C_{carb}$ and $\delta^{18}O$ of carbonates using a Multicarb inlet device in-line with a 253 plus isotope ratio mass spectrometer (Spötl, 2011). The $CO_2$ analyte gas was separated using gas chromatography, and $H_2O$ was eliminated using a Nafion trap before being admitted into the mass spectrometer equipped with a continuous flow interface. The international standard NBS-19 was utilized and calibrated to the Vienna Pee Dee Belemnite (V-PDB) scale. The analytical uncertainties for most samples were less than ±0.05‰ for $\delta^{13}C_{carb}$ and $\delta^{18}O$ based on standard analyses and ±0.1‰ based on the reproducibility of replicate analyses.

The fine-grained powders were acidified by 3 M HCl to thoroughly eliminate the carbonate component, and the percentages of calcite were then determined by utilizing these residues. The carbonate-free residues were dried overnight in an oven. The content and isotopic values of organic carbon and TN were analysed via combustion to $CO_2$ and $N_2$ using an EA Isolink series elemental analyser interfaced with a 253 plus isotope ratio mass spectrometer (IRMS). A proper amount of the residues (1~25 mg) was transferred into a tin capsule and further introduced into a quartz combustion column at 1040 °C. Subsequently, $CO_2$ and $N_2$ entered the IRMS via He carrier gas. The $N_2$ and $CO_2$ isotopic ratios are reported in delta notation in per mil (‰) relative to atmospheric $N_2$ and Pee Dee Belemnite (PDB), respectively. Two carbon isotope standards (urea: $\delta^{13}C = -28.25‰ \pm 0.24‰$) were inserted for each set of 10 samples, and the tested carbon isotopes of the standards generated a precision within 0.2‰. The uncertainties were generally better than 0.4‰ based on the reproducibility of replicate carbon isotopic analyses of samples. Two nitrogen isotopic standards (International standard IVA33802153: $\delta^{15}N = +5.78 \pm 0.1‰$) were inserted for each set of 10 samples, and the tested nitrogen isotopes of the standards generated a precision within 0.2‰. Uncertainties based on the reproducibility of replicate nitrogen isotopic analyses were less than 0.3‰. The TOC and TN abundances were calculated by multiplying the percentages of carbon and nitrogen with the percentage of residue after acidification.

Trace element abundances were tested using a Thermo Scientific Element XR inductively coupled plasma mass spectrometer (ICP–MS). A proper amount of the homogenized residues (~40 mg) was reacted with a mixture of $HNO_3$ + HCl + HF in a

https://doi.org/10.1017/S0016756823000833 Published online by Cambridge University Press

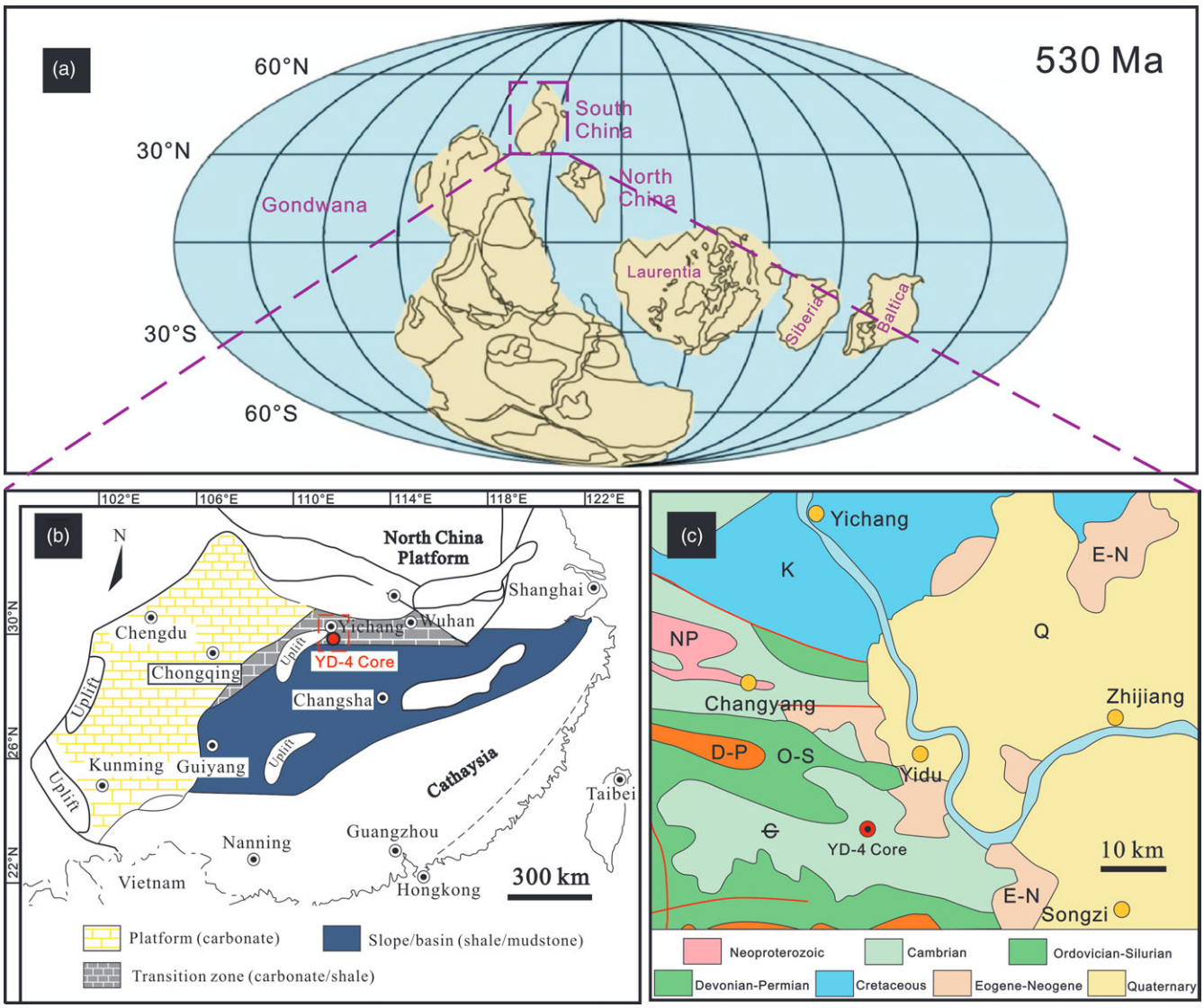


**Figure 1.** (Colour online) (a) Early Cambrian paleogeography (~530 Ma; adapted from Li *et al.* 2008); (b) paleogeographic reconstruction of the South China Craton during the earliest Cambrian, with the position of the YD-4 borehole presented in the red box (modified from Cremonese *et al.* 2013); (c) geological map of the study area (modified from Chen *et al.* 2018).

sealed Teflon cup. The Chinese national standards GSR1 (granite) and GSR3 (basalt) were employed for the purpose of uncertainty detection. The analytical precision was better than 2%.

## 4. Results

Our high-resolution chemostratigraphic results are presented in Fig. 2 and recorded in Table 1. The TOC abundances from the YD-4 core are typically low, with values in the range of 0.01 to 0.06% in the uppermost Dengying Formation and the lower part of the Yanjiahe Formation, followed by an increasing trend in the middle part of the Yanjiahe Formation (up to 2.54%) and then reaching a peak as high as 16.47% in the overlying Shuijingtuo Formation. Bulk carbonate $\delta^{13}C$ analyses display a negative shift from 2.14‰ in the Dengying and basal Yanjiahe formations to −3.86‰ in the middle part of the Yanjiahe Formation, and then the values increase to 1.45‰ over the next 2 m. Within the basal Shuijingtuo Formation, the $\delta^{13}C_{carb}$ values reach a nadir of ca. −5.47‰. The carbonate oxygen isotopes reveal much less short-term variability in the upper part of the Dengying Formation, with an average of −6‰, and then drop to −10‰ in the middle part of the Yanjiahe Formation followed by a 2% positive excursion in the overlying layers. The $\delta^{13}C_{org}$ profile shows relatively stable values of approximately −29‰ in the Dengying Formation and a smooth negative shift close to −34.4‰ in the middle part of the Yanjiahe Formation. After a recovery of values to −29.8‰ at the top of the Yanjiahe Formation, another negative signal occurs at the boundary with the Shuijingntuo Formation.

The TN abundances increase steadily up section from approximately 10 ppm in the Denying Formation to higher values, reaching 709 ppm in the Yanjiahe Formation, and then the values continuously increase to peak values of approximately 2000 ppm in the Shuijingtuo Formation. The $\delta^{15}N$ values increase upward from high values of approximately 3.3‰ in the uppermost Dengying Formation to a low value of 0.3‰ in the middle part of the Shuijingtuo Formation; then, the values increase to 4.0‰ over the next 2 m before decreasing monotonically to −1‰ in the upper part of the Yanjiahe and the overlying Shuijingtuo Formation. The C/N values span a range of 5.4

https://doi.org/10.1017/S0016756823000833 Published online by Cambridge University Press

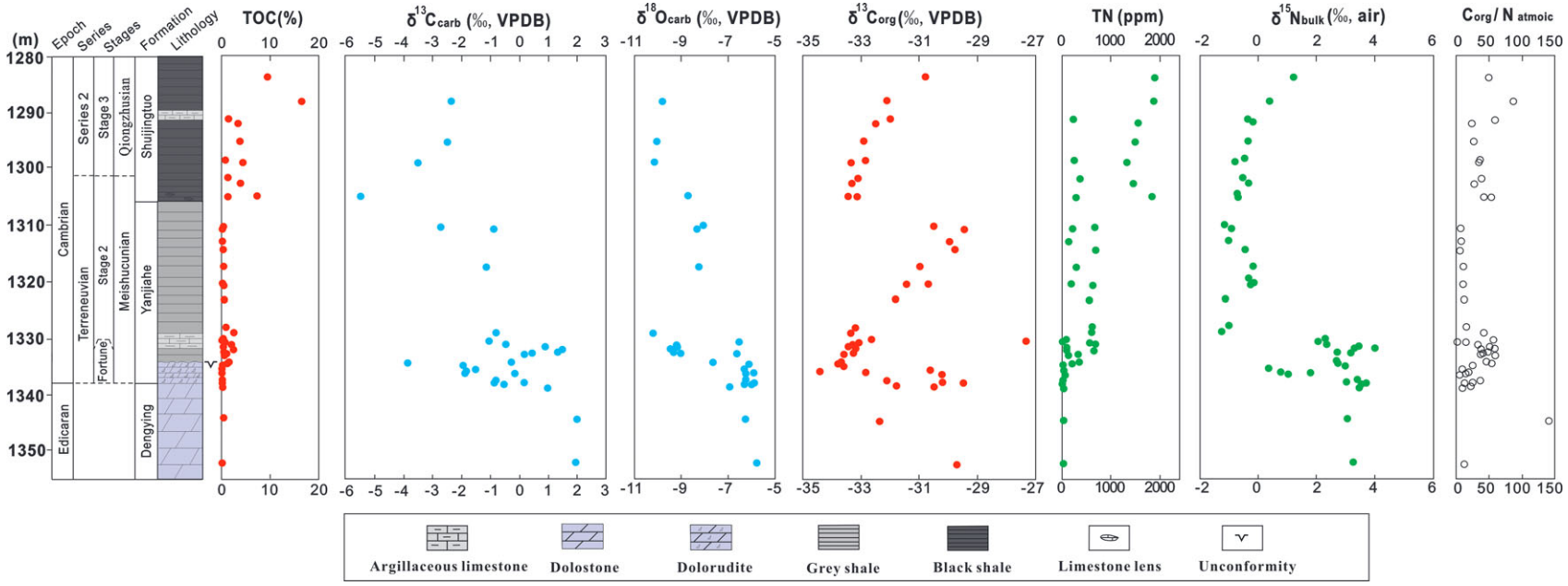


**Figure 2.** (Colour online) Depth profile showing the lithostratigraphic, isotopic and elemental information from the YD-4 borehole in the Yangtze Block.

**Table 1.** Chemostratigraphic data from the YD-4 core

| Depth/m | Formation | Lithology | Carbonate/% | $\delta^{15}N$/‰ | TN/$10^{-6}$ | TOC/% | $\delta^{13}C_{org}$/‰ | $\delta^{13}C_{carb}$/‰ | $\delta^{18}O$/‰ | $C_{org}/N$ | Mn/ppm | Sr/ppm | Mn/Sr |
|---|---|---|---|---|---|---|---|---|---|---|---|---|---|
| 1283.6 | Shuijingtuo | Shale | 21.50 | 1.21 | 1888.17 | 9.43 | −30.78 | | | 49.94 | 316 | 818 | 0.39 |
| 1287.9 | Shuijingtuo | Shale | 17.80 | 0.39 | 1874.83 | 16.47 | −32.13 | | | 87.85 | | | |
| 1291.2 | Shuijingtuo | Limestone | 90.11 | −0.36 | 239.69 | 1.40 | −31.97 | −2.34 | −9.80 | 58.43 | 355 | 510 | 0.70 |
| 1291.9 | Shuijingtuo | Shale | 18.82 | −0.20 | 1537.83 | 3.57 | −32.47 | | | 23.19 | 355 | 315 | 1.13 |
| 1295.1 | Shuijingtuo | Shale | 21.65 | −0.34 | 1493.13 | 3.90 | −32.88 | | | 26.11 | 373 | 255 | 1.46 |
| 1298.5 | Shuijingtuo | argillaceous Limestone | 87.63 | −0.50 | 255.89 | 0.90 | −32.85 | −2.48 | −10.04 | 35.00 | 262 | 441 | 0.59 |
| 1299 | Shuijingtuo | Shale | 23.63 | −0.81 | 1330.67 | 4.40 | −33.35 | | | 33.07 | 336 | 285 | 1.18 |
| 1301.7 | Shuijingtuo | argillaceous Limestone | 77.73 | −0.53 | 361.01 | 1.38 | −33.11 | −3.51 | −10.14 | 38.33 | 358 | 509 | 0.70 |
| 1302.6 | Shuijingtuo | Shale | 15.95 | −0.34 | 1457.17 | 3.95 | −33.32 | | | 27.12 | 266 | 191 | 1.39 |
| 1304.8 | Shuijingtuo | Shale | 9.19 | −0.73 | 1829.77 | 7.57 | −33.45 | | | 41.35 | 191 | 115 | 1.66 |
| 1305 | Shuijingtuo | Limestone lens | 85.67 | −0.71 | 274.56 | 1.45 | −33.12 | −5.47 | −8.67 | 52.90 | 657 | 109 | 6.03 |
| 1310.3 | Yanjiahe | Shale | 28.56 | −1.15 | 673.94 | 0.37 | −30.48 | | | 5.42 | 247 | 152 | 1.63 |
| 1310.7 | Yanjiahe | Limestone | 67.87 | −0.92 | 238.90 | 0.15 | −29.44 | −2.72 | −8.07 | 6.09 | 512 | 353 | 1.45 |
| 1312.9 | Yanjiahe | Limestone | 76.96 | −0.99 | 139.15 | 0.10 | −29.97 | −0.90 | −8.33 | 7.27 | 504 | 397 | 1.27 |
| 1314.5 | Yanjiahe | Shale | 23.30 | −0.43 | 709.25 | 0.31 | −29.75 | | | 4.43 | 204 | 167 | 1.22 |
| 1317.4 | Yanjiahe | Shale | 52.96 | −0.18 | 304.25 | 0.32 | −30.97 | | | 10.38 | 332 | 192 | 1.73 |
| 1320.4 | Yanjiahe | Limestone | 77.18 | −0.16 | 194.64 | 0.16 | −30.69 | −1.13 | −8.25 | 8.23 | 618 | 380 | 1.63 |
| 1320.7 | Yanjiahe | Shale | 33.97 | −0.28 | 633.12 | 0.63 | −31.43 | | | 10.00 | 204 | 170 | 1.20 |
| 1323.3 | Yanjiahe | Shale | 29.15 | −1.10 | 556.36 | 0.60 | −31.82 | | | 10.76 | 216 | 176 | 1.23 |
| 1328.1 | Yanjiahe | Shale | 28.18 | −0.99 | 616.83 | 0.92 | −33.17 | | | 14.91 | 200 | 181 | 1.10 |
| 1329.2 | Yanjiahe | Shale | 25.77 | −1.23 | 610.77 | 2.54 | −33.34 | | | 41.55 | 179 | 165 | 1.08 |
| 1330.3 | Yanjiahe | argillaceous Limestone | 93.65 | 2.29 | 72.76 | 0.41 | −32.64 | −0.82 | −10.18 | 56.21 | 136 | 218 | 0.62 |
| 1330.9 | Yanjiahe | Shale | 32.05 | 2.06 | 571.10 | 0.85 | −33.08 | | | 14.81 | 162 | 1200 | 0.14 |
| 1331.2 | Yanjiahe | Shale | 30.70 | 2.36 | 666.85 | 2.13 | −33.29 | | | 31.90 | 247 | 1566 | 0.16 |
| 1331.6 | Yanjiahe | argillaceous Limestone | 90.88 | 3.45 | 77.65 | 0.40 | −33.40 | −0.49 | −9.21 | 51.08 | 80 | 257 | 0.31 |
| 1331.9 | Yanjiahe | argillaceous Limestone | 90.55 | 3.29 | 80.87 | 0.47 | −33.19 | 0.88 | −9.16 | 57.76 | 85 | 267 | 0.32 |
| 1332 | Yanjiahe | Shale | 29.90 | 4.00 | 655.61 | 2.42 | −33.25 | | | 36.84 | 160 | 1205 | 0.13 |
| 1332.6 | Yanjiahe | phosphate limestone | 85.86 | 2.67 | 89.40 | 0.43 | −33.28 | 1.45 | −9.43 | 48.34 | 85 | 318 | 0.27 |
| 1332.7 | Yanjiahe | phosphate Limestone | 80.54 | 3.18 | 110.17 | 0.45 | −33.26 | 1.31 | −9.31 | 41.16 | 89 | 292 | 0.30 |
| 1332.8 | Yanjiahe | Shale | 53.90 | 2.73 | 333.38 | 1.23 | −33.60 | | | 36.87 | 181 | 380 | 0.48 |
| 1333 | Yanjiahe | Shale | 80.21 | 3.21 | 131.86 | 0.77 | −33.56 | 0.43 | −9.00 | 58.45 | 297 | 174 | 1.71 |

(*Continued*)

**Table 1.** (*Continued*)

| | | | | | | | | | | | | | |
|---|---|---|---|---|---|---|---|---|---|---|---|---|---|
| 1334.3 | Yanjiahe | siliceous Dolorudite | 51.32 | 2.70 | 357.38 | 1.66 | −33.68 | 0.17 | −6.61 | 46.40 | 152 | 316 | 0.48 |
| 1334.6 | Yanjiahe | siliceous Dolorudite | 77.02 | 2.75 | 217.41 | 1.16 | −33.79 | −0.30 | −7.63 | 53.27 | 215 | 226 | 0.95 |
| 1334.9 | Yanjiahe | siliceous Dolorudite | 93.68 | 2.90 | 17.08 | 0.04 | −33.59 | −3.86 | −6.11 | 23.78 | 383 | 474 | 0.81 |
| 1335.7 | Yanjiahe | Dolorudite | 89.09 | 0.35 | 38.04 | 0.03 | −30.61 | −1.94 | −6.09 | 8.21 | 161 | 81 | 1.99 |
| 1336 | Yanjiahe | Dolorudite | 90.52 | 0.78 | 43.69 | 0.08 | −34.40 | −1.51 | −6.30 | 18.52 | 208 | 220 | 0.95 |
| 1336.2 | Yanjiahe | Dolorudite | 90.11 | 1.79 | 37.60 | 0.05 | −32.85 | −1.83 | −5.90 | 14.24 | 165 | 88 | 1.88 |
| 1336.5 | Yanjiahe | Dolorudite | 83.67 | 1.03 | 61.17 | 0.02 | −30.19 | −1.86 | −5.91 | 3.94 | 424 | 1755 | 0.24 |
| 1330.7 | Yanjiahe | Dolorudite | 41.92 | | | 0.02 | −27.32 | −0.15 | −6.27 | | 163 | 69 | 2.36 |
| 1337.6 | Yanjiahe | Dolorudite | 98.87 | 3.40 | 14.73 | 0.05 | −32.12 | −1.04 | −6.52 | 35.98 | 156 | 161 | 0.97 |
| 1337.9 | Dengying | Dolomilite | 98.04 | 3.02 | 7.95 | 0.02 | −30.21 | −0.80 | −6.26 | 23.54 | 138 | 93 | 1.48 |
| 1338.1 | Dengying | Dolomilite | 99.47 | 3.73 | 3.01 | 0.00 | −29.47 | 0.14 | −5.87 | 12.30 | 163 | 57 | 2.86 |
| 1338.4 | Dengying | Dolomilite | 99.60 | 3.59 | 5.00 | 0.01 | −31.77 | −0.86 | −6.26 | 21.13 | 132 | 42 | 3.14 |
| 1338.9 | Dengying | Dolomilite | 99.19 | 3.48 | 12.44 | 0.01 | −30.48 | −0.55 | −6.00 | 9.09 | 148 | 67 | 2.21 |
| 1344.6 | Dengying | Dolomilite | 98.43 | 3.10 | 25.56 | 0.36 | −32.34 | 0.96 | −6.93 | 141.73 | 142 | 118 | 1.20 |
| 1352.3 | Dengying | Dolomilite | 98.51 | 3.26 | 4.26 | 0.00 | −29.71 | 1.99 | −6.23 | 11.13 | 123 | 47 | 2.62 |
| 1357.5 | Dengying | Dolomilite | 98.33 | 2.50 | 12.27 | 0.01 | −28.04 | 1.94 | −5.78 | 6.80 | 123 | 68 | 1.81 |

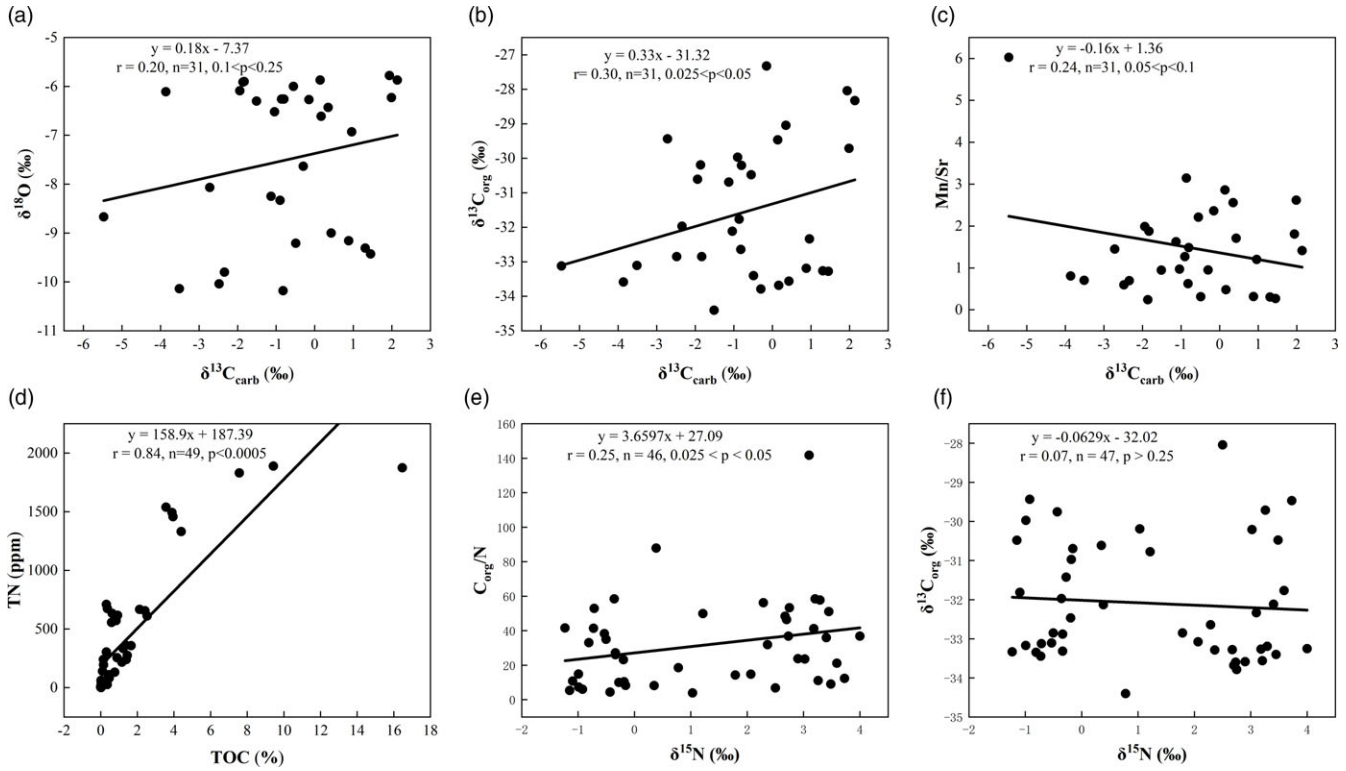


**Figure 3.** (Colour online) Crossplots of $\delta^{13}C_{carb}$ vs. $\delta^{18}O$ (a), $\delta^{13}C_{org}$ vs. $\delta^{13}C_{carb}$ (b), $\delta^{13}C_{carb}$ vs. Mn/Sr (c), TOC vs. TN (d), $\delta^{15}N$ vs. $C_{org}/N_{bulk}$ (e) and $\delta^{13}C_{org}$ vs. $\delta^{15}N$ (f) from the YD-4 borehole. The data are presented in Table 1.

to 141.7, with peaks corresponding to the middle part of the Yanjiahe Formation and the Shuijingtuo shale.

## 5. Discussion

### 5.a. Diagenesis

To estimate the diagenetic effect of meteoric water-derived fluids on the study areas, geochemical criteria are applied. The $\delta^{18}O$ of carbonate is considered an effective proxy for diagenesis because high oxygen concentrations in diagenetic fluid can significantly affect $\delta^{18}O$ (Knauth & Kennedy, 2009; Derry, 2010). Typically, $\delta^{18}O$ values <−10‰ may present an altered $\delta^{13}C_{carb}$ composition (e.g., Kah, 2000). Our data show that the $\delta^{18}O$ values range from −5.2‰ to −10.8‰, with an average of −7.5‰, implying that the $\delta^{13}C_{carb}$ composition from the YD-4 core probably preserves the primary signal. The noncoincidental observations between $\delta^{13}C_{carb}$ and $\delta^{18}O$ ($r = 0.20$, $n = 31$, $0.1 < p < 0.25$) in the studied samples may also represent a primary cause rather than diagenesis (Fig. 3a). Indeed, a slight correlation between $\delta^{13}C_{carb}$ and $\delta^{13}C_{org}$ in the samples ($r = 0.30$, $n = 31$, $0.025 < p < 0.05$, Fig. 3b) supports this view due to the different diagenetic effects on organic and inorganic carbon (Knoll *et al.* 1986). In addition, as meteoric or burial diagenesis normally raises Mn concentrations and lowers Sr concentrations, Mn/Sr values can also be considered valid proxies for evaluating diagenesis (Veizer, 1983). In carbonate samples, a Mn/Sr ratio lower than 10 is regarded as indicative of the original $\delta^{13}C_{carb}$ composition (Kaufman & Knoll, 1995). The Mn/Sr values in this study range from 0.1 to 2.9, with an average of 1.3 (Table 1), suggesting weak diagenetic alteration. This result is also in line with the lack of a correlation between $\delta^{13}C_{carb}$ and the Mn/Sr ratio ($r = 0.24$, $n = 31$, $0.05 < r < 0.1$, Fig. 3c).

Postdepositional influence can also result in the alteration of nitrogen abundance and possible $\delta^{15}N$. We found that the TOC and TN abundances in this study are positively correlated ($r = 0.84$, $n = 46$, $p < 0.0005$, Fig. 3d), indicating a great contribution of organic molecules to TN samples. In the early diagenetic stage, preferential degradation of $^{14}N$-enriched materials (proteins and nucleic acids, etc.) could lead to a slight decrease in the C/N ratio and an increase in the isotopic value of organic nitrogen (Lehmann *et al.* 2002). In addition, if the samples have been influenced by thermal alteration associated with metamorphism, a selective removal of isotopically light N and C and a positive correlation between $\delta^{15}N$ and $\delta^{13}C_{org}$ would be expected (Busigny *et al.* 2003; Rivera *et al.* 2015). However, no clear correlations between $\delta^{15}N$ values, C/N ratios and $\delta^{13}C_{org}$ values are observed in this study (Fig. 3e and 3f), indicating that the $\delta^{15}N$ composition of the YD-4 core samples was not remarkably influenced by burial fluids.

### 5.b. Regional stratigraphic correlation

Due to discrete fossil and chronological data, carbon isotope curves are the most reliable tool for correlations of data in the E-C transition. Although the comparisons of $\delta^{13}C$ stratigraphic curves demonstrate spatial heterogeneity in the Yangtze Block (Okada *et al.* 2014; Chen *et al.* 2019), which was probably associated with the poor communication between the shallow water and the outer sea or with the missing Cambrian strata, a broad correlation has been shown in previous cases (e.g., Yuan *et al.* 2014; Jin *et al.* 2016; Wang *et al.* 2018). To trace carbon isotope anomalies that are closely related to the evolution of Cambrian fauna in the cores in this study and to evaluate the possible link between environmental evolution and biological events during the early Cambrian, the

https://doi.org/10.1017/S0016756823000833 Published online by Cambridge University Press

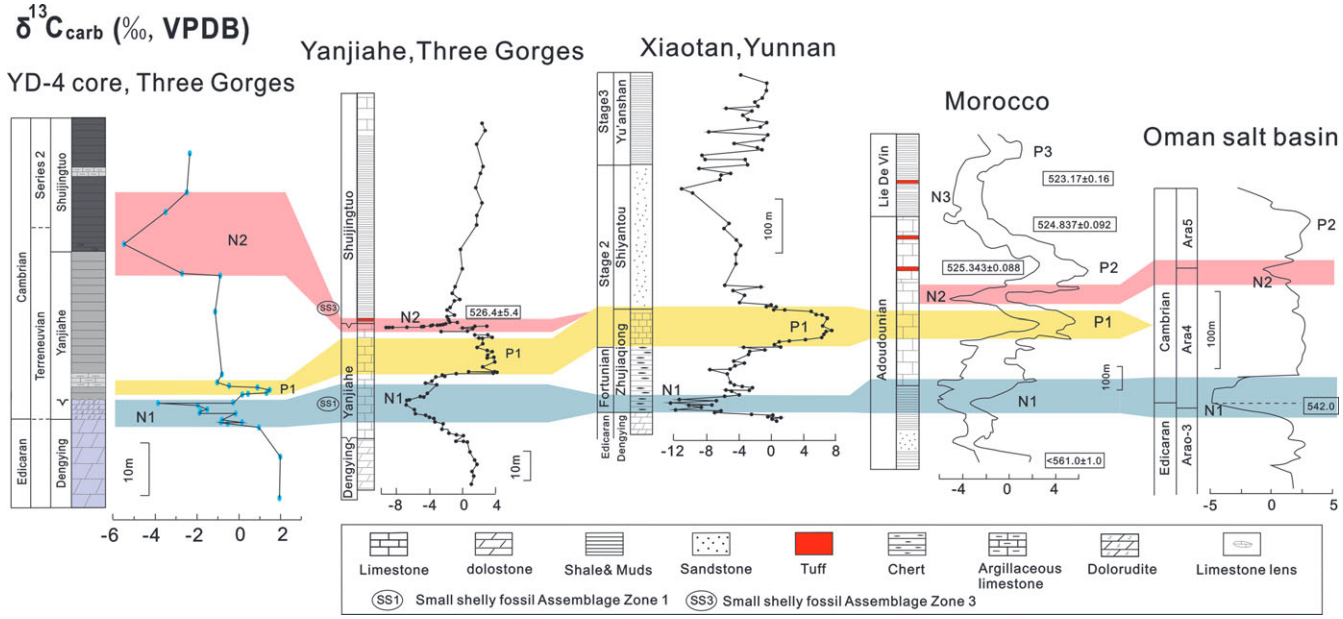


**Figure 4.** (Colour online) Stratigraphic correlation framework comparing the section in this study, the Yanjiahe section (Ishikawa *et al*. 2008; Okada *et al*. 2014), the Xiaotan section (Cremonese *et al*. 2013) and the Morocco section (Maloof *et al*. 2010).

correlations of the stratigraphic framework in typical sections of the Yangtze Block as well as larger regions should be considered.

Many well-preserved outcrops that contain the E-C boundary have been observed in the Yangtze Block. Ishikawa *et al*. (2008) conducted a high-precision carbon isotope chemostratigraphic study in the Yanjiahe section, which is situated in the Three Gorges area. The general features of the carbon isotope evolution curves obtained from our samples are generally comparable with those from the Yanjiahe section (Fig. 4). There are at least two negative carbonate carbon isotope anomalies (N1 and N2) and one positive anomaly (P1) that can be identified in the study section. The first negative $\delta^{13}C_{carb}$ excursion of ~5‰ (N1) occurred in the lower part of the Yanjiahe Formation at the beginning of the Cambrian, and this negative shift can also be correlated with that in the contemporaneous successions in the Xiaotan section (Fig. 4), as well as the Meishucun (Brasier *et al*. 1990) and Laolin (Shen & Schidlowski, 2000) sections. However, the minimum of ~−4‰ in our drill core study is moderately higher than that from other sections. This discrepancy might result from multiple reasons, including the sampling resolution and/or diagenetic effect. In addition, SSF assemblages are irreplaceable for correlations of the *pretrilobitic* Cambrian (Terreneuvian). Previous works have evaluated the SSF associations of the Yanjiahe Formation in several typical sections of Yanjiahe village in the Three Gorges area. The Yanjiahe Formation, in turn, contains the *A. trisulcatus–P. anabarica* assemblage zone, the *P. antiqua* assemblage zone and the *A. yanjiaheensis* assemblage zone (Chen, 1984; Steiner *et al*. 2007; Guo *et al*. 2014), implying that the Yanjiahe Formation is early to mid-Meishucunian in age. However, SSF associations of the Yanjiahe Formation were reported from other outcrops in the Three Gorges area, rather than from the present study core. Microscopic observations of YD-4 core samples showed only a few SSF assemblages (Cao *et al*., 2023), which failed to establish a continuous evolutionary association of SSF assemblages. Due to certain limitations in studying biostratigraphy based on core samples, we admit that there is uncertainty regarding the age of the lower part of the study section. Instead, we can only pay more attention from the perspectives of stratigraphic constraints and comparable carbon isotope stratigraphy. In the stratigraphic sequence of the YD-4 core, the dolorudite of the Yanjiahe Formation conformably contacts the underlying dolomite of the Dengying Formation. Thus, N1 in the YD-4 core is the first positive excursion at the base of the Cambrian. Analogously, in the Xiaotan section, a conformable contact is recognized between the Dengying Formation and the overlying Zhujiaqiong Formation, and the first negative excursion at the base of the Cambrian is believed to be the Basal Cambrian Carbon Isotope Excursion (BACE, negative $\delta^{13}C$ values, Cremonese *et al*. 2013). Thus, we speculate that the N1 event recognized in the lower part of the Yanjiahe Formation in this study core may correspond to the BACE.

Globally, many profiles also have the characteristic $\delta^{13}C$ excursion that began in the terminal Ediacaran and reached the lowest point at the basal E-C boundary, including in Morocco (Maloof *et al*. 2010, see Fig. 4), the Mackenzie Mountains in NE Canada (Narbonne *et al*. 1994), the Anabar Platform in NE Siberia (Kaufman *et al*. 1996) and SW Mongolia (Brasier *et al*. 1996). These layers all document the first occurrence of the SSF assemblage, and thus, this negative $\delta^{13}C_{carb}$ excursion event is also considered a global marker of the E-C boundary. Note that the tuffaceous bed in Oman provided a U–Pb age of 542 ± 0.3 Ma (Amthor *et al*. 2003), which is consistent with the lowest $\delta^{13}C_{carb}$ value, further confirming the global carbon cycling response at the E-C boundary.

In the YD-4 records, the $\delta^{13}C$ values show another rapid negative excursion reaching −9‰ (N2) across the boundary of the Yanjiahe-Shuijingtuo formations. The nano-SIMS U–Pb age of the base of the Shuijingtuo Formation in the Three Gorges area was estimated to be 526.4 ± 5.4 Ma (Okada *et al*. 2014). A previous study showed that the Shuijingtuo Formation was characterized by *Hupeidiscus* and *Tsunyidiscus* (Xue & Zhou 2006), and Zhu *et al*. (2003) also recognized the Atdabanian stage-type *trilobites* in the upper part of the Shuijingtuo Formation (Zhu *et al*. 2003). Trilobites first occurred at the base of the Shuijingtuo Formation (Guo *et al*. 2014), suggesting that the lower part of the Shuijingtuo Formation likely coincides with the latest Meishucunian age, which

https://doi.org/10.1017/S0016756823000833 Published online by Cambridge University Press

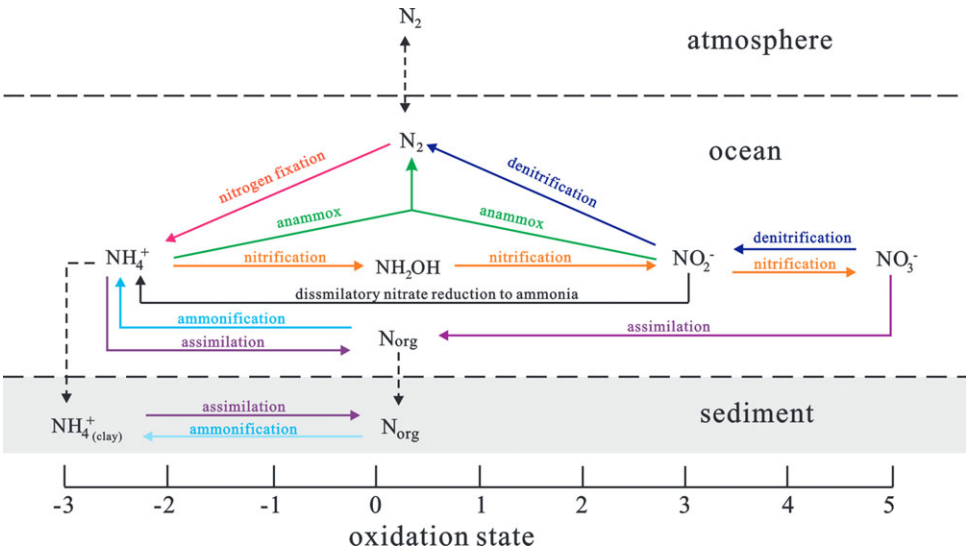


**Figure 5.** (Colour online) Application of the modern nitrogen cycle to the early Cambrian marine environment. For an analysis of dominant pathways in the lower Cambrian, see the main text. Modified from Godfrey and Falkowski (2009).

is comparable to the Tommotian age of the Siberian platform (Kouchinsky *et al.* 2012). Moreover, such a large negative isotope excursion (~5‰ in this study) was reported in the Xiaotan, Morocco and Oman sections (Fig. 4), suggesting a global perturbation of the seawater carbon cycle. Based on the chemo- and biostratigraphic evidence and the conformable contact between the Yanjiahe and Shuijingtuo formations in the Three Gorges area, we speculate that the N2 event recognized across the Yanjiahe and Shuijingtuo Formation boundary corresponds to the Shiyantou Carbon Isotope Excursion (SHICE, negative $\delta^{13}C$ values) that developed during the latest Cambrian Stage 2.

A positive excursion of +6‰ in the middle part of the Yanjiahe Formation was detected in the study core (P1). High-resolution carbon isotope evidence shows that the Zhujiaqing Carbon Isotope Excursion (ZHUCE, positive $\delta^{13}C$ values) was the last positive excursion in the continuous carbon isotope perturbations between the BACE and the SHICE during the early Cambrian period (Ren *et al.* 2019). Combined with chemostratigraphic information of the Yanjiahe Formation, the P1 event in this study core can be correlated with the ZHUCE in the lower part of Cambrian Stage 2. This carbon isotope anomaly also exists in other sections in the Yangtze Block, such as the Xiaotan (Fig. 4), Meishucun (Brasier *et al.* 1990), Maidiping (Brasier *et al.* 1990) and Laolin (Shen & Schidlowski, 2000) sections. However, the feature of P1 in the YD-4 core is defined as a shorter duration and a lower maximum $\delta^{13}C$ value (~1.5‰) relative to other sections, which are probably due to an unconformity between the dolorudite and the overlying dark shale of the Yanjiahe Formation in the study area.

### 5.c. Evaluation of δ15N signals during the earliest Cambrian

Nitrogen cycle patterns in the modern ocean are important for revealing the nitrogen biogeochemical pathways preserved in sedimentary rocks (Fig. 5). The most significant source of biological nitrogen in the ocean comes from nitrogen fixation, which enzymatically converts atmospheric $N_2$ into biologically available nitrogen ($NH_4^+$) through diazotrophy (mainly cyanobacteria) (Sigman *et al.* 2009). The most common nitrogenase enzyme for nitrogen fixation (e.g., Mo- and Fe-based enzymes) induces only a minor isotope fractionation of approximately −1‰ ($\varepsilon_{product\text{-}reactan}$ = −2‰ to 1‰) (Stüeken *et al.* 2016). Direct assimilation of $NO_3^-$ and $NH_4^+$ is another way to capture biologically available nitrogen in the ocean, and incomplete assimilation of $NH_4^+$ and $NO_3^-$ can yield isotopic fractionations of ~−4‰ to −27‰ and −5‰ to −10‰, respectively (Vo *et al.* 2013; Casciotti, 2009). However, this scenario occurs only under extremely high nutrient levels, for instance, eutrophication conditions at high latitudes and upwelling systems in the equatorial Pacific Ocean (Sigman *et al.* 2009).

The removal of fixed nitrogen from seawater is mainly determined by denitrification and anaerobic ammonium oxidation (anammox), which are both active in suboxic environments and appear today primarily in oxygen minimum zones (OMZs) and oxygen-depleted pore waters (Sigman *et al.* 2009; Hong *et al.* 2019). Denitrification can normally convert $NO_3^-$ by anaerobic bacteria to $N_2$ and lead to a residual nitrate reservoir enriched in heavier $^{15}N$ with fractionation values of −20 ~ −30‰ (Brandes & Devol, 2002). The isotopic fractionation of anammox can also reach up to −25‰ (Prokopenko *et al.* 2006). Moreover, it was experimentally demonstrated that individual steps in nitrification can also amplify the fractionations in oxic water columns; however, net isotopic fractionation is normally not expressed via this pathway because nitrification is usually quantitatively associated with its fast rate of reaction (Lipschultz *et al.* 1990). Thus, the primary $\delta^{15}N$ composition is finally determined by the equilibrium between nitrogen fixation and denitrification/anammox, and this parameter also includes reliable redox clues.

Given the buildup of $\delta^{13}C_{carb}$ in the stratigraphic correlation framework, the BACE, ZHUCE and SHICE events have been recognized in the study area, where the BACE is coupled to a significant negative $\delta^{15}N$ excursion (down to +0.3‰, Fig. 2). These values are distinctly lower than those from the modern ocean nitrate pool of ~+5‰ (Sigman & Casciotti, 2001) and thus are suggested to be a strengthened nitrogen fixation signal. Environmentally controlled experiments have shown that only when seawater nitrate is consumed quantitatively at the chemocline can diazotrophy balance the nutrient structure of seawater by increasing nitrogen fixation (Sigman *et al.* 2009). Given that denitrification and anammox are anaerobic nitrogen cycling processes, the $^{15}N$-depleted isotopic signal associated with a slightly increasing TOC trend (up to 2.5%) might be independently explained by expanded marine anoxia in the

https://doi.org/10.1017/S0016756823000833 Published online by Cambridge University Press

earliest Cambrian Yangtze Sea. This scenario resembles the nitrogen isotope signal preserved in the Cretaceous Oceanic Anoxic Event (Higgins *et al.* 2012) and Late Devonian Hangenberg Event (Liu *et al.* 2016). Analogously, the SHICE across the boundary of the Yanjiahe and Shuijingtuo formations is marked by decreasing trends of $\delta^{13}C_{carb}$ and $\delta^{13}C_{org}$ values accompanied by relatively long-term low $\delta^{15}N$ values at approximately −1‰. We propose that the lighter $\delta^{15}N$ values in the SHICE would result from an insufficient nitrate pool and intensified atmospheric nitrogen fixation, as well as partial ammonium assimilation into biomass (e.g., Liu *et al.* 2013; Liu *et al.* 2020).

The ZHUCE in this study coincides with a rapidly increasing $\delta^{15}N$ trend (up to 4.0‰), which is closer to the mean nitrogen isotope value of nitrate in modern open-ocean environments, implying that the nitrogen cycle experienced a key fluctuation during deposition of the lowermost Yanjiahe Formation. Based on the differences in net fractionation between sedimentary denitrification (~−1 to −3‰) and water-column denitrification, reservoir box modelling emphasized that secular variation in the $\delta^{15}N$ of sediments was dependent on the dominant locus of denitrification (Algeo *et al.* 2014). However, there is still controversy over the interpretation of paleoclimate and paleoenvironmental models for different nitrogen isotope distributions and their corresponding dominant locus of denitrification (Junium & Arthur, 2007; Liu *et al.* 2008), which may be related to differences in timescales and/or restriction of marine basins (Algeo *et al.* 2014). Accepting that nitrogen fixation and denitrification are considered two main end members that affect the nitrogen isotope pattern of nitrate, we propose that the ~4‰ positive excursion in $\delta^{15}N$ was likely a consequence of declined rates of denitrification and a deepening chemocline, thereby amplifying the oxic water mass associated with an elevated nitrate pool. However, the $\delta^{15}N$ value increased to only 4.0‰, which is still slightly below the levels found in modern oceans, implying that the nitrate pool of surface water in the ZHUCE was lower than the current level.

### 5.d. Implication for early Cambrian biotic evolution

Several carbon isotope anomalies closely related to the evolution of early Cambrian life have been identified, implying temporal coupling between the prosperity/extinction of organisms and marine environmental changes (Zhu *et al.* 2007; Betts *et al.* 2018; George *et al.* 2021; Topper *et al.* 2022). For example, the diversification of Ediacaran fauna can be correlated to the Dengying Positive Carbon Isotope Excursion (DEPCE, negative $\delta^{13}C$ values); the extinction of the Ediacaran fauna near the E-C boundary on a global scale is synchronous with the BACE; the rapid radiation of the SSF assemblages in Cambrian Stage 2 can be well correlated with the ZHUCE; the extinction of the SSFs in Cambrian Stage 2 corresponds to the SHICE and the initial explosion of arthropods (especially trilobites) corresponds to the Cambrian Arthropod Radiation Isotope Excursion (CARE, positive $\delta^{13}C$ values) (Fig. 6).

The remarkable increase in dissolved oxygen levels in oceans was thought to serve as a pivotal catalyst that resulted in the innovation of primitive simple animals and their diversification (e.g., Erwin *et al.* 2011; Sperling *et al.* 2013). Indeed, the two negative $\delta^{15}N$ excursions in this study occur synchronously in the BACE and SHICE, indicating the impact of the expansion of anoxic water masses on the living environment of the Ediacaran fauna and small shelly fauna. The BACE has a wide global response (Maloof *et al.* 2010; Zhu *et al.* 2019), and its initiation is coincident with sea level rise (Ishikawa *et al.* 2014). Iron speciation information provided evidence of anoxic and ferruginous environments in the Lower and Upper Yangtze areas during the E-C transition, such as the Diben section of Zhejiang, Silikou section of northern Guangxi and Longbizui and Yanwutan sections of western Hunan (Chang *et al.* 2010; Wang *et al.* 2012; Yuan *et al.* 2014). Given that the Rodinia breakup and Gondwana amalgamation occurred during the E-C transition, ocean circulation induced by plate movement might have led to enhanced upwelling on continental margins (Tucker, 1992; Wille *et al.* 2008; Ader *et al.* 2014; Wang *et al.* 2015). In this case, deep-water upwelling would have enhanced nutrient fluxes and transported $^{13}C$-depleted anoxic water masses to the shallow platform area. In the ZHUCE, the $\delta^{15}N$ value (with a maximum of 4‰) is slightly smaller than that of the modern ocean, indicating that the degree of oxidation was highly associated with the deepening chemocline, which provided a favorable $O_2$ demand for the radiation of the small shelly fauna. The $\delta^{15}N$ returned to 0~−2‰ in the SHICE, which is indicative of the shallower chemocline relative to that in the BACE. The lower $\delta^{15}N$ value in the SHICE is consistent with the largest global marine transgression during the Phanerozoic associated with strong upwelling (Goldberg *et al.* 2007), which would have transported the reducing deep water to the shallow-water area, thereby leading to the temporal extinction of small shelly fauna.

On the other hand, changes in the bioavailable nitrogen pool may have exerted an important influence on the regulation of eukaryotic organisms because oceanic nitrate is the preferential source of nitrogen for eukaryotic organisms (Karl *et al.* 2001). The variability in the oceanic nitrate pool mainly depends on the aerobic and anaerobic nitrogen cycling paths (Lehmann *et al.* 2002). Increased fixed nitrogen supply and episodic animal radiation have been proposed based on the coupling relationship between long-term $\delta^{15}N$ variations and major diversifications in the metazoan group, as documented by body fossil and biomarker records (Wang *et al.* 2018; Wu *et al.* 2022). Contraction of the oceanic nitrate pool was associated with an anaerobic N cycle when the ocean became more anoxic with a shallower chemocline in the BACE and SHICE. Such nitrate limitation could have been linked to lower primary productivity and delayed radiation of eukaryotic organisms (e.g., Anbar & Knoll, 2002; Koehler *et al.* 2017). The aerobic N cycle and more abundant nitrate available in the surface water are shown in the ZHUCE, which could have been beneficial to the evolution from single-celled microorganisms toward a eukaryote-dominated community (e.g., Stüeken, 2013; Wang *et al.* 2018).

## 6. Conclusions

Time-series carbon and nitrogen isotopic data obtained from the YD-4 core samples across the E-C transition in the Yangtze Block present a sequence of significant disturbances, offering valuable environmental insights for the evolution of eukaryotes in the middle Yangtze Block. According to the comparison of the $\delta^{13}C_{carb}$ curves from several representative sections in the Yangtze Block and other time-equivalent strata in other larger regions, the BACE, ZHUCE and SHICE are well constrained in the study area. Within the BACE and SHICE in the transitional facies in the middle Yangtze Block, the $\delta^{15}N$ value displays a rapidly negative excursion (~0‰), suggesting enhanced microbial nitrogen fixation and partial ammonium assimilation, which were likely linked to complete denitrification associated with expanded anoxic conditions. In contrast, the positive $\delta^{15}N$ values in the ZHUCE

https://doi.org/10.1017/S0016756823000833 Published online by Cambridge University Press

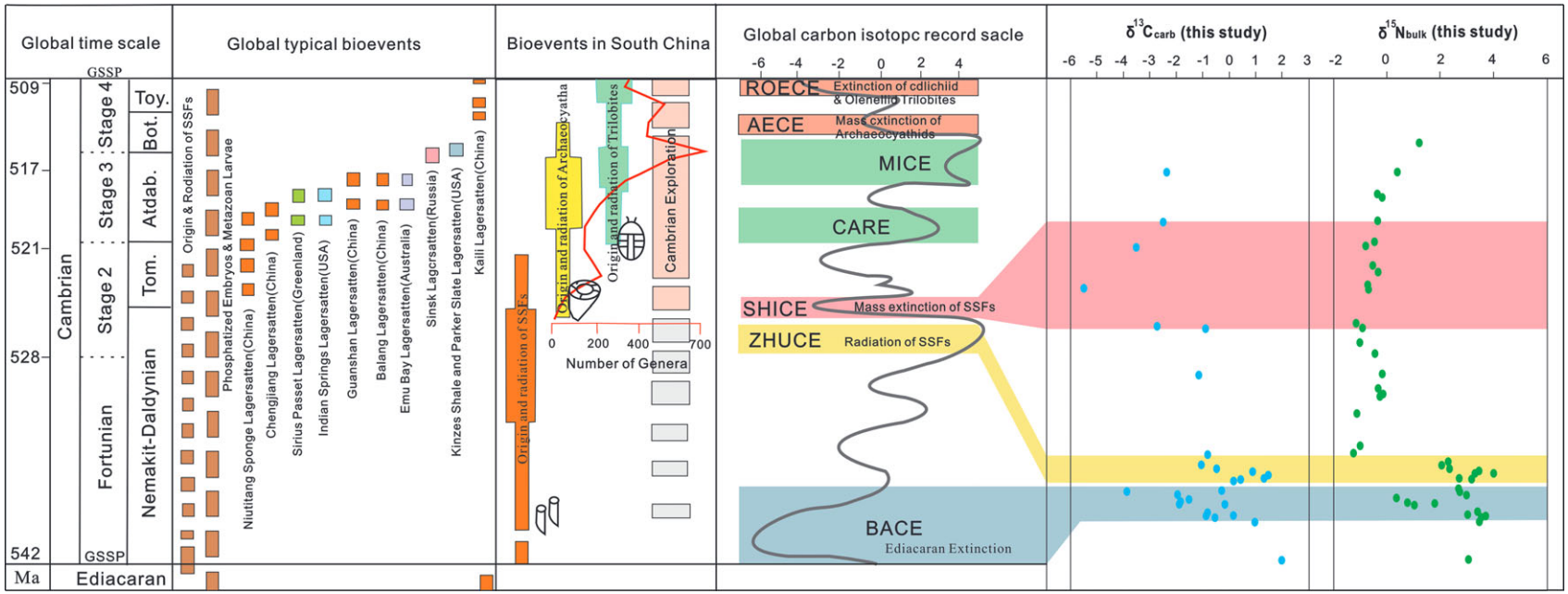


**Figure 6.** (Colour online) Compilation of evolutionary events with $\delta^{13}C_{carb}$ values during the early Cambrian (modified from Ren *et al*. 2019). The diversity data of animal genera are from Li *et al*. (2007) and the $\delta^{13}C_{carb}$ curves are from Zhu *et al*. (2006).

indicate a growing nitrate pool with a deeper chemocline. Given the linkage between the carbon isotope anomaly events and the $\delta^{15}N$ patterns, the widespread anoxic water conditions may have been related to the extinction of Cambrian-type animals, while an expansion of oxic waters and an amplified nitrate pool in the surface waters may have promoted Cambrian biodiversity.

**Acknowledgments.** We are grateful for support from the China Geological Survey (DD20230006), the Natural Science Foundation of Hubei Province (2023AFB1103), Guangdong Natural Science Foundation of China (2022A1515012100), the Foreign Aid Project of the Ministry of Commerce of the People's Republic of China ((2021) 28), South China Sea Scholar Project of Guangdong Ocean University (002029002007), Guangdong Provincial College Innovation Team Project (2019KCXTF021) and First-class Discipline Plan of Guangdong Province (080503032101, 231420003).

## References

**Ader M, Sansjofre P, Halverson GP, Busigny V, Trindade RI, Kunzmann M and Nogueira AC** (2014) Ocean redox structure across the Late Neoproterozoic Oxygenation Event: a nitrogen isotope perspective. *Earth Planetary Science Letters* **396**, 1–13.

**Algeo TJ and Li C** (2020) Environmental analysis of paleoceanographic systems based on molybdenum–uranium covariation. *Chemical Geology* **268**, 211–25.

**Algeo TJ, Meyers PA, Robinson RS, Rowe H and Jiang GQ** (2014) Icehouse–greenhouse variations in marine denitrification. *Biogeosciences* **11**, 1273–95.

**Algeo TJ and Tribovillard N** (2009) Trace-element behavior and redox facies in core shales of Upper Pennsylvanian Kansas-type cyclothems. *Chemical geology* **206**, 289–318.

**Amthor JE, Grotzinger JP, Schröder S, Bowring SA, Ramezani J, Martin MW and Matter A** (2003) Extinction of Cloudina and Namacalathus at the Precambrian-Cambrian boundary in Oman. *Geology* **31**, 431–4.

**Anbar AD and Knoll AH** (2002) Proterozoic ocean chemistry and evolution: a bioinorganic bridge? *Science* **297**, 1137–42.

**Betts MJ, Paterson JR, Jacquet SM, Andrew AS, Hall PA, Jago JB, Jagodzinski EA, Preiss WV, Crowley JL and Brougham T** (2018) Early Cambrian chronostratigraphy and geochronology of South Australia. *Earth-Science Reviews* **185**, 498–543.

**Brandes JA and Devol AH** (2002) A global marine-fixed nitrogen isotopic budget: implications for Holocene nitrogen cycling. *Global Biogeochemical Cycles* **16**, 1–14.

**Brasier M, Shields G, Kuleshov V and Zhegallo E** (1996) Integrated chemo- and biostratigraphic calibration of early animal evolution: neoproterozoic–early Cambrian of southwest Mongolia. *Geological Magazine* **133**, 445–85.

**Brasier MD, Magaritz M, Corfield R, Huilin L, Xiche W, Lin O, Zhiwen J, Hamdi B, Tinggui H and Fraser AG** (1990) The carbon-and oxygen-isotope record of the Precambrian–Cambrian boundary interval in China and Iran and their correlation. *Geological Magazine* **127**, 319–32.

**Busigny V, Cartigny P, Philippot P, Ader M and Javoy M** (2003) Massive recycling of nitrogen and other fluid-mobile elements (K, Rb, Cs, H) in a cold slab environment: evidence from HP to UHP oceanic metasediments of the Schistes Lustrés nappe (western Alps, Europe). *Earth Planetary Science Letters* **215**, 27–42.

**Canfield DE, Glazer AN and Falkowski PG** (2010) The evolution and future of earth's nitrogen cycle. *Science* **330**, 192–6.

**Canfield DE, Poulton SW, Knoll AH, Narbonne GM, Ross G, Goldberg T and Strauss H** (2008) Ferruginous conditions dominated later Neoproterozoic deep-water chemistry. *Science* **321**, 949–52.

**Cao HS, Wang ZY, Dong LF, Xiao YC, Hu LM, Chen FJ, Wei K, Chen CQ, Song ZG, Wu L** (2023) Influence of hydrothermal and upwelling events on organic matter accumulation in the gas-bearing lower Cambrian shales of the middle Yangtze Block, South China. *Marine and Petroleum Geology* **155**, 106373.

**Casciotti KL** (2009) Inverse kinetic isotope fractionation during bacterial nitrite oxidation. *Geochimica et Cosmochimica Acta* **73**, 2061–76.

**Chang H, Chu X, Feng L and Huang J** (2010) Iron speciation in cherts from the Laobao Formation, South China: implications for anoxic and ferruginous deep-water conditions. *Chinese Science Bulletin* **55**, 3189–96.

**Chang H, Chu X, Feng L, Huang J and Chen Y** (2018) Marine redox stratification on the earliest Cambrian (ca. 542–529 Ma) Yangtze platform. *Palaeogeography, Palaeoclimatology, Palaeoecology* **504**, 75–85.

**Chen J-Y** (2009) The sudden appearance of diverse animal body plans during the Cambrian explosion. *International Journal of Developmental Biology* **53**, 733–51.

**Chen L, Zhang B, Jiang S, Chen X, Zhang G, Zhang J, Wei W, Lu Y, Chen P and Lin W** (2022) Provenance, source weathering, and tectonic setting of the lower Cambrian Shuijingtuo formation in the Middle Yangtze area, China. *Marine Petroleum Geology* **139**, 105584.

**Chen P** (1984) Discovery of Lower Cambrian small shelly fossils from Jijiapo, Yichang, west Hubei and its significance. *Professional papers of Stratigraphy Palaeontology* **13**, 49–66.

**Chen X, We K, Zhang B, Li P, Li H, Liu A and Luo S** (2018) Main geological factors controlling shale gas reservior in the Cambrian Shuijingtuo Formation in Yichang of Hubei Province as well as its and enrichment patterns. *Geology in China* **45**, 207–26.

**Chen Y, Diamond CW, Stüeken EE, Cai C, Gill BC, Zhang F, Bates SM, Chu X, Ding Y and Lyons TW** (2019) Coupled evolution of nitrogen cycling and redoxcline dynamics on the Yangtze Block across the Ediacaran-Cambrian transition. *Geochimica et Cosmochimica Acta* **257**, 243–65.

**Clarkson M, Poulton S, Guilbaud R and Wood R** (2014) Assessing the utility of Fe/Al and Fe-speciation to record water column redox conditions in carbonate-rich sediments. *Chemical Geology* **382**, 111–22.

**Cremonese L, Shields-Zhou G, Struck U, Ling H-F, Och L, Chen X and Li D** (2013) Marine biogeochemical cycling during the early Cambrian constrained by a nitrogen and organic carbon isotope study of the Xiaotan section, South China. *Precambrian Research* **225**, 148–65.

**Derry LA** (2010) On the significance of $\delta^{13}C$ correlations in ancient sediments. *Earth Planetary Science Letters* **296**, 497–501.

**Devol AH** (2015) Denitrification, anammox, and $N_2$ production in marine sediments. *Annual Review of Marine Science* **7**, 403–23.

**Erwin DH, Laflamme M, Tweedt SM, Sperling EA, Pisani D and Peterson KJ** (2011) The Cambrian conundrum: early divergence and later ecological success in the early history of animals. *Science* **334**, 1091–7.

**Fan H, Wen H, Han T, Zhu X, Feng L and Chang H** (2018) Oceanic redox condition during the late Ediacaran (551–541 Ma), South China. *Geochimica et Cosmochimica Acta* **238**, 343–56.

**Fu D, Tong G, Dai T, Liu W, Yang Y, Zhang Y, Cui L, Li L, Yun H and Wu Y** (2019) The Qingjiang biota—a Burgess Shale–type fossil Lagerstätte from the early Cambrian of South China. *Science* **363**, 1338–42.

**Gao P, Liu G, Jia C, Young A, Wang Z, Wang T, Zhang P and Wang D** (2016) Redox variations and organic matter accumulation on the Yangtze carbonate platform during Late Ediacaran–Early Cambrian: constraints from petrology and geochemistry. *Palaeogeography, Palaeoclimatology, Palaeoecology* **450**, 91–110.

**George BG, Kumar S and Ray JS** (2021) C-Sr isotope stratigraphy of carbonate formations of the late Neoproterozoic-Cambrian Marwar Supergroup, western India. *Precambrian Research* **364**, 106378.

**Godfrey LV and Falkowski PG** (2009) The cycling and redox state of nitrogen in the Archaean ocean. *Nature Geoscience* **2**, 725–9.

**Goldberg T, Strauss H, Guo Q and Liu C** (2007) Reconstructing marine redox conditions for the Early Cambrian Yangtze Platform: evidence from biogenic sulphur and organic carbon isotopes. *Palaeogeography, Palaeoclimatology, Palaeoecology* **254**, 175–93.

**Guo J, Li Y and Li G** (2014) Small shelly fossils from the early Cambrian Yanjiahe Formation, Yichang, Hubei, China. *Gondwana Research* **25**, 999–1007.

**Higgins MB, Robinson RS, Husson JM and Pearson A** (2012) Dominant eukaryotic export production during ocean anoxic events reflects the importance of recycled $NH_4^+$. *Proceedings of the National Academy of Sciences of the United States of America* **109**, 2269–74.

**Hong Y, Wu J, Guan F, Yue W and Long A** (2019) Nitrogen removal in the sediments of the Pearl River Estuary, China: evidence from the distribution and forms of nitrogen in the sediment cores. *Marine Pollution Bulletin* **138**, 115–24.

**Ishikawa T, Ueno Y, Komiya T, Sawaki Y, Han J, Shu D, Li Y, Maruyama S and Yoshida N** (2008) Carbon isotope chemostratigraphy of a Precambrian/Cambrian boundary section in the Three Gorge area, South China: prominent global-scale isotope excursions just before the Cambrian Explosion. *Gondwana Research* **14**, 193–208.

**Ishikawa T, Ueno Y, Shu D, Li Y, Han J, Guo J, Yoshida N, Maruyama S and Komiya T** (2014) The $\delta^{13}C$ excursions spanning the Cambrian explosion to the Canglangpuian mass extinction in the Three Gorges area, South China. *Gondwana Research* **25**, 1045–56.

**Jiang G, Wang X, Shi X, Xiao S, Zhang S and Dong J** (2012) The origin of decoupled carbonate and organic carbon isotope signatures in the early Cambrian (ca. 542–520 Ma) Yangtze platform. *Earth and Planetary Science Letters* **317**, 96–110.

**Jin C, Li C, Algeo TJ, Planavsky NJ, Cui H, Yang X, Zhao Y, Zhang X and Xie S** (2016) A highly redox-heterogeneous ocean in South China during the early Cambrian (~529–514 Ma): implications for biota-environment co-evolution. *Earth and Planetary Science Letters* **441**, 38–51.

**Jin C, Li C, Algeo TJ, Wu S, Cheng M, Zhang Z and Shi W** (2020) Controls on organic matter accumulation on the early-Cambrian western Yangtze Platform, South China. *Marine and Petroleum Geology* **111**, 75–87.

**Junium CK and Arthur MA** (2007) Nitrogen cycling during the Cretaceous, Cenomanian-Turonian Oceanic Anoxic Event II. *Geochemistry Geophysics Geosystems* **8**, 1–18.

**Kah LC** (2000) Preservation of depositional δ18O signatures in Proterozoic dolostones: Geochemical constraints on seawater chemistry and early diagenesis. In *Deposition and Diagenesis in an Evolving Precambrian World* (eds JP Grotzinger and NP James), vol. 67, pp. 245–360. SEPM Special Publication.

**Karl D, Bidigare R and Letelier R** (2001) Long-term changes in plankton community structure and productivity in the North Pacific Subtropical Gyre: the domain shift hypothesis. *Deep Sea Research Part II: Topical Studies in Oceanography* **48**, 1449–70.

**Kaufman AJ and Knoll AH** (1995) Neoproterozoic variations in the C-isotopic composition of seawater: stratigraphic and biogeochemical implications. *Precambrian Research* **73**, 27–49.

**Kaufman AJ, Knoll AH, Semikhatov MA, Grotzinger JP, Jacobsen SB and Adams W** (1996) Integrated chronostratigraphy of Proterozoic–Cambrian boundary beds in the western Anabar region, northern Siberia. *Geological Magazine* **133**, 509–33.

**Knauth LP and Kennedy MJ** (2009) The late Precambrian greening of the Earth. *Nature* **460**, 728–32.

**Knoll A, Hayes J, Kaufman A, Swett K and Lambert I** (1986) Secular variation in carbon isotope ratios from Upper Proterozoic successions of Svalbard and East Greenland. *Nature* **321**, 832–8.

**Koehler MC, Stüeken EE, Kipp MA, Buick R and Knoll AH** (2017) Spatial and temporal trends in Precambrian nitrogen cycling: A Mesoproterozoic offshore nitrate minimum. *Geochimica et Cosmochimica Acta* **198**, 315–37.

**Kouchinsky A, Bengtson S, Runnegar B, Skovsted C, Steiner M and Vendrasco M** (2012) Chronology of early Cambrian biomineralization. *Geological Magazine* **149**, 221–51.

**Laflamme M, Darroch SAF, Tweedt SM, Peterson KJ and Erwin DH** (2013) The end of the Ediacara biota: Extinction, biotic replacement, or Cheshire Cat? *Gondwana Research* **23**, 558–73.

**Lehmann MF, Bernasconi SM, Barbieri A and McKenzie JA** (2002) Preservation of organic matter and alteration of its carbon and nitrogen isotope composition during simulated and in situ early sedimentary diagenesis. *Geochimica et Cosmochimica Acta* **66**, 3573–84.

**Lenton TM, Boyle RA, Poulton SW, Shields-Zhou GA and Butterfield NJ** (2014) Co-evolution of eukaryotes and ocean oxygenation in the Neoproterozoic era. *Nature Geoscience* **7**, 257–65.

**Li C, Zhang Z, Jin C, Cheng M, Wang H, Huang J and Algeo TJ** (2020) Spatiotemporal evolution and causes of marine euxinia in the early Cambrian Nanhua Basin (South China). *Palaeogeography, Palaeoclimatology, Palaeoecology* **546**, 109676.

**Li G, Steiner M, Zhu X, Yang A, Wang H and Erdtmann BD** (2007) Early Cambrian metazoan fossil record of South China: Generic diversity and radiation patterns. *Palaeogeography, Palaeoclimatology, Palaeoecology* **254**, 229–49.

**Li Z-X, Bogdanova S, Collins A, Davidson A, De Waele B, Ernst RE, Fitzsimons ICW, Fuck RA, Gladkochub DP, Jacobs J, Karlstrom KE, Lu S, Natapov LM, Pease V, Pisarevsky SA, Thrane K and Vernikovsky V** (2008) Assembly, configuration, and break-up history of Rodinia: a synthesis. *Precambrian Research* **160**, 179–210.

**Lipschultz F, Wofsy S, Ward B, Codispoti L, Friedrich G and Elkins J** (1990) Bacterial transformations of inorganic nitrogen in the oxygen-deficient waters of the Eastern Tropical South Pacific Ocean. Deep Sea Research Part A. *Oceanographic Research Papers* **37**, 1513–41.

**Liu J, Qie W, Algeo TJ, Yao L, Huang J and Luo G** (2016) Changes in marine nitrogen fixation and denitrification rates during the end-Devonian mass extinction. *Palaeogeography, Palaeoclimatology, Palaeoecology* **448**, 195–206.

**Liu K-K, Kao S-J, Chiang K-P, Gong G-C, Chang J, Cheng J-S and Lan C-Y** (2013) Concentration dependent nitrogen isotope fractionation during ammonium uptake by phytoplankton under an algal bloom condition in the Danshuei estuary, northern Taiwan. *Marine Chemistry* **157**, 242–52.

**Liu Y, Magnall JM, Gleeson SA, Bowyer F, Poulton SW and Zhang J** (2020) Spatio-temporal evolution of ocean redox and nitrogen cycling in the early Cambrian Yangtze ocean. *Chemical Geology* **554**, 119803.

**Liu Z, Altabet MA and Herbert TD** (2008.) Plio-Pleistocene denitrification in the eastern tropical North Pacific: intensification at 2.1Ma. *Geochemistry Geophysics Geosystems* **9**, 1–14.

**Maloof AC, Ramezani J, Bowring SA, Fike DA, Porter SM and Mazouad M** (2010) Constraints on early Cambrian carbon cycling from the duration of the Nemakit-Daldynian–Tommotian boundary $\delta^{13}C$ shift, Morocco. *Geology* **38**, 623–6.

**Marshall CR** (2006) Explaining the Cambrian "explosion" of animals. *Annual Review of Earth & Planetary Sciences* **34**, 355–84.

**Mills DB and Canfield DE** (2014) Oxygen and animal evolution: did a rise of atmospheric oxygen "trigger" the origin of animals? *BioEssays* **36**, 1145–55.

**Narbonne GM, Kaufman AJ and Knoll AH** (1994) Integrated chemostratigraphy and biostratigraphy of the Windermere Supergroup, northwestern Canada: implications for Neoproterozoic correlations and the early evolution of animals. *Geological Society of America Bulletin* **106**, 1281–92.

**Och LM, Cremonese L, Shields-Zhou GA, Poulton SW, Struck U, Ling H, Li D, Chen X, Manning C and Thirlwall M** (2016) Palaeoceanographic controls on spatial redox distribution over the Yangtze Platform during the Ediacaran–Cambrian transition. *Sedimentology* **63**, 378–410.

**Okada Y, Sawaki Y, Komiya T, Hirata T, Takahata N, Sano Y, Han J and Maruyama S** (2014) New chronological constraints for Cryogenian to Cambrian rocks in the Three Gorges, Weng'an and Chengjiang areas, South China. *Gondwana Research* **25**, 1027–44.

**Prokopenko M, Hammond D, Berelson W, Bernhard J, Stott L and Douglas R** (2006) Nitrogen cycling in the sediments of Santa Barbara basin and Eastern Subtropical North Pacific: nitrogen isotopes, diagenesis and possible chemosymbiosis between two lithotrophs (Thioploca and Anammox)—"riding on a glider". *Earth and Planetary Science Letters* **242**, 186–204.

**Ren Y, Zhong D, Gao C, Li B, Cao X, Wang A, Dong Y and Yan T** (2019) The paleoenvironmental evolution of the Cambrian Longwangmiao Formation (Stage 4, Toyonian) on the Yangtze Platform, South China: Petrographic and geochemical constrains. *Marine and Petroleum Geology* **100**, 391–411.

**Rivera KT, Puckette J and Quan TM** (2015) Evaluation of redox versus thermal maturity controls on $\delta^{15}N$ in organic rich shales: a case study of the Woodford Shale, Anadarko Basin, Oklahoma, USA. *Organic Geochemistry* **83**, 127–39.

**Shen Y and Schidlowski M** (2000) New C isotope stratigraphy from southwest China: Implications for the placement of the Precambrian-Cambrian boundary on the Yangtze Platform and global correlations. *Geology* **28**, 623–6.

**Sigman DM and Casciotti K** (2001) Nitrogen isotopes in the ocean. *Encyclopedia of Ocean Sciences* **3**, 1884–94.

**Sigman DM, Karsh KL and Casciotti KL** (2009) Nitrogen isotopes in the ocean. In *Encyclopedia of Ocean Sciences* (eds JH Steele, SA Thorpe and KK Turekian), pp. 40–54. Oxford: Academic Press.

https://doi.org/10.1017/S0016756823000833 Published online by Cambridge University Press

**Sperling EA, Frieder C, Raman AV, Girguis PR, Levin LA and Knoll AH** (2013) Oxygen, ecology, and the Cambrian radiation of animals. *Proceedings of the National Academy of Sciences* **110**, 13446–51.

**Spötl C** (2011) Long-term performance of the Gasbench isotope ratio mass spectrometry system for the stable isotope analysis of carbonate micro-samples. *Rapid Communications in Mass Spectrometry* **25**, 1683–1685.

**Steiner M, Li G, Qian Y, Zhu M and Erdtmann B-D** (2007) Neoproterozoic to early Cambrian small shelly fossil assemblages and a revised biostratigraphic correlation of the Yangtze Platform (China). *Palaeogeography, Palaeoclimatology, Palaeoecology* **254**, 67–99.

**Stüeken EE** (2013) A test of the nitrogen-limitation hypothesis for retarded eukaryote radiation: Nitrogen isotopes across a Mesoproterozoic basinal profile. *Geochimica et Cosmochimica Acta* **120**, 121–39.

**Stüeken EE, Kipp MA, Koehler MC and Buick R** (2016) The evolution of earth's biogeochemical nitrogen cycle. *Earth-Science Reviews* **160**, 220–39.

**Topper T, Betts MJ, Dorjnamjaa D, Li G, Li L, Altanshagai G, Enkhbaatar B and Skovsted CB** (2022) Locating the BACE of the Cambrian: Bayan Gol in southwestern Mongolia and global correlation of the Ediacaran–Cambrian boundary. *Earth-Science Reviews* **229**, 104017.

**Tucker ME** (1992) The Precambrian–Cambrian boundary: seawater chemistry, ocean circulation and nutrient supply in metazoan evolution, extinction and biomineralization. *Journal of the Geological Society* **149**, 655–68.

**Veizer J** (1983) Trace elements and isotopes in sedimentary carbonates. *Reviews in Mineralogy* **11**, 265–300.

**Vo J, Inwood W, Hayes JM and Kustu S** (2013) Mechanism for nitrogen isotope fractionation during ammonium assimilation by Escherichia coli K12. *Proceedings of the National Academy of Sciences* **110**, 8696–701.

**Wang D, Ling H-F, Struck U, Zhu X-K, Zhu M, He T, Yang B, Gamper A and Shields GA** (2018) Coupling of ocean redox and animal evolution during the Ediacaran-Cambrian transition. *Nature Communications* **9**, 2575.

**Wang D, Struck U, Ling H-F, Guo Q-J, Shields-Zhou GA, Zhu M-Y and Yao S-P** (2015) Marine redox variations and nitrogen cycle of the early Cambrian southern margin of the Yangtze Platform, South China: evidence from nitrogen and organic carbon isotopes. *Precambrian Research* **267**, 209–26.

**Wang J, Chen D, Yan D, Wei H and Xiang L** (2012) Evolution from an anoxic to oxic deep ocean during the Ediacaran–Cambrian transition and implications for bioradiation. *Chemical Geology* **306**, 129–38.

**Wang J and Li Z-X** (2003) History of Neoproterozoic rift basins in South China: implications for Rodinia break-up. *Precambrian Research* **122**, 141–58.

**Wei G-Y, Ling H-F, Li D, Wei W, Wang D, Chen X, Zhu X-K, Zhang F-F and Yan B** (2017) Marine redox evolution in the early Cambrian Yangtze shelf margin area: evidence from trace elements, nitrogen and sulphur isotopes. *Geological Magazine* **154**, 1344–59.

**Wille M, Nägler TF, Lehmann B, Schröder S and Kramers JD** (2008) Hydrogen sulphide release to surface waters at the Precambrian/Cambrian boundary. *Nature* **453**, 767–9.

**Wu Y, Tian H, Jia W, Li J, Li T, Zhou Q and Xie L** (2022) Nitrogen isotope evidence for stratified ocean redox structure during late Ediacaran to Cambrian Age 3 in the Yangtze Block of South China. *Chemical Geology* **589**, 120679.

**Xiao S** (2012) Oxygen and early animal evolution, *AGU Fall Meeting Abstracts*, B54B–08.

**Xue Y and Zhou C** (2006) Resedimentation of the Early Cambrian phosphatized small shell fossils and correlation of the Sinian–Cambrian boundary strata in the Yangtze Region, southern China. *Journal of Stratigraphy* **30**, 64–74.

**Yuan Y, Cai C, Wang T, Xiang L, Jia L and Chen Y** (2014) Redox condition during Ediacaran–Cambrian transition in the Lower Yangtze deep water basin, South China: constraints from iron speciation and $\delta^{13}$Corg in the Diben section, Zhejiang. *Chinese Science Bulletin* **59**, 3638–49.

**Zhang JF, Xu H, Zhou Z, Ren PF, Guo JZ and Wang Q** (2019) Geological characteristics of shale gas reservoir in Yichang area, western Hubei. *Acta Petrologica Sinica* **40**, 887–99.

**Zhu G, Wang P, Li T, Zhao K, Yan H, Li J and Zhou L** (2021) Nitrogen geochemistry and abnormal mercury enrichment of shales from the lowermost Cambrian Niutitang formation in South China: implications for the marine redox conditions and hydrothermal activity. *Global and Planetary Change* **199**, 103449.

**Zhu M, Yang A, Yuan J, Li G, Zhang J, Zhao F, Ahn S-Y and Miao L** (2019) Cambrian integrative stratigraphy and timescale of China. *Science China Earth Sciences* **62**, 25–60.

**Zhu M, Zhang J and Yang A** (2007) Integrated Ediacaran (Sinian) chronostratigraphy of South China. *Palaeogeography, Palaeoclimatology, Palaeoecology* **254**, 7–61.

**Zhu M, Zhang J, Yang A, Li G, Steiner M and Erdtmann BD** (2003) Sinian-Cambrian stratigraphic framework for shallow-to deep-water environments of the Yangtze platform: an integrated approach. *Progress in Natural Science* **13**, 951–60.

**Zhu M-Y, Babcock LE and Peng S-C** (2006) Advances in Cambrian stratigraphy and paleontology: Integrating correlation techniques, paleobiology, taphonomy and paleoenvironmental reconstruction. *Palaeoworld* **15**, 217–222.

**Zhuravlev AY and Wood RA** (2018) The two phases of the Cambrian explosion. *Scientific Reports* **8**, 1–10.